Supplementary information: quasi-particle tunneling across an exciton condensate

Ding Zhang[1,2], Joseph Falson[2], Stefan Schmult[2], Werner Dietsche[2], and Jurgen H. Smet[2]

[1]*State Key Laboratory of Low-Dimensional Quantum Physics and Department of Physics, Tsinghua University, Beijing 100084, China*

[2]*Max Planck Institute for Solid State Research, Heisenbergstrasse 1, D-70569 Stuttgart, Germany*

(Dated: May 6, 2020)

Abstract

In the supplementary information, we present simulation results of the potential profile and density in the region of the quantum point contact (QPC). We also discuss the key transport quantities derived from the Landauer-Büttiker formalism and include additional data sets of the tunnel conductance near $\nu_{tot} = 1$ for two different QPCs.

SIMULATION OF THE QUANTUM POINT CONTACT

Figure S1 shows the Hall bar structure together with the split gates that define the quantum point contact (QPC). The split gates have a nominal separation of 4 μm. They are vertically displaced from the quantum wells by a spacer of approximately 710 nm. As a result of this large separation, the orifice of the quantum point contact potential of the two-dimensional electron gas (2DEG) is much narrower. To simulate this narrowing, 3D self-consistent Poisson calculations were carried out with the nextnano software (nextnano GmbH). Figure S2 displays the modeled structure and the calculated results. The real wafer contains in-situ grown LT-GaAs and multiple superlattices on the substrate. This complex heterostructure is simplified to the symmetric geometry shown in Fig. S2. To minimize the computation time, the doping levels used were obtained by first running 1D self-consistent Poisson-Schrödinger tests until the density values in the two quantum wells match experimental values in the balanced case [Fig. S2(a)]. In the following simulation, we study the influence of top gates on this heterostructure. A gate voltage of -0.5 V is applied to the two top gates to simulate the depletion effect brought about by the work function difference between the metallic gates and the semiconductor.

Close to the center ($x = 0, y = 0$) of the QPC, the split gates do not affect the 2DEG. Hence, the conduction band profile along the z-direction at $x, y = 0$ reflects the band structure in the bulk. Fig. S2 (c) shows 2D colored plots of the density distribution. The top and bottom panels are slices at the top and bottom quantum well, while the middle panel illustrates the vertical density distribution. From these plots it is apparent that the QPC opening in the top layer is narrower than in the bottom layer.

In order to assess the effective width of the QPC, the percentage density change in the upper and lower quantum well is plotted in panel (d) of Fig. S2. Starting from the center of the QPC and moving to the region beneath the gate, the density drops down to zero and the relative density change approaches 100%. Although full depletion is only reached underneath the gate, a wide region not covered by the gate is affected. In the balanced case the $\nu_{tot} = 1$ quantum Hall state only tolerates a small density variation. Fig. S3 plots the longitudinal resistance in the vicinity of the $\nu_{tot} = 1$ state for different total densities, i.e. different degrees of layer-imbalance. At higher backgate voltage, the total density is increased and the $\nu_{tot} = 1$ state occurs at higher magnetic field. This shift to higher fields is

accompanied by a reduction of the width of the longitudinal resistance minimum signaling the $\nu_{tot} = 1$ state. We estimate this width (ΔB) from the distance between the vertical dotted bars. The density tolerance, defined as $\Delta n/n_{tot}$, is proportional to $\Delta B/B_0$ (B_0 is the central magnetic field of the $\nu_{tot} = 1$ state). Figure S3(b) shows that $\Delta n/n_{tot}$ decreases with increasing total density. For the balanced case at a total density of 5.44×10^{10} cm^{-2}, the $\nu_{tot} = 1$ state only tolerates a relative density change of up to 1.5%. The resistance trace corresponding to the balanced case is also plotted as an inset to panel (d) of Fig. S2. The dotted vertical line in Fig. S2(d) marks the region within the QPC where the $\nu_{tot} = 1$ survives. Regions with a relative density change larger than 1.5% become insulating at this magnetic field. The opening of the QPC in the 2DEG is therefore effectively about 2.4 μm in the balanced regime. More generally, when applying higher backgate voltages the QPC opening narrows.

LANDAUER-BÜTTIKER FORMALISM

Applying the Landauer-Büttiker formalism to our measurement configuration yields the following equations:

$$R_D = \frac{h}{e^2}\frac{1}{\nu_{QPC}}, \tag{1}$$

$$R_D^- = -\frac{h}{e^2}\left(\frac{2}{\nu_{bulk}} - \frac{1}{\nu_{QPC}}\right), \tag{2}$$

$$R_T = \frac{h}{e^2}\left(\frac{1}{\nu_{QPC}} - \frac{1}{\nu_{bulk}}\right). \tag{3}$$

R_D (R_D^-) refers to the diagonal resistance value for $B > 0$ ($B < 0$). R_T is the longitudinal resistance across the QPC. The difference between R_D and $|R_D^-|$ reflects the chirality of the edge current. This can be further verified by comparing $(R_D + |R_D^-|)/2$ with R_{xy}. From the equations, we find:

$$\frac{R_D + |R_D^-|}{2} = \frac{h}{\nu_{bulk} e^2}. \tag{4}$$

As shown in the main text, although R_D and R_D^- are measured at opposite magnetic fields, $(R_D + |R_D^-|)/2$ simply collapses back to R_{xy} in the quantum Hall regime. This overlapping behavior supports the existence of edge channels in this quantum Hall bilayer system.

In Fig. S4, we also show data of the same sample, but measured in a different refrigerator. There, not only R_D, R_D^-, but also R_T was measured. This was one of the early measurements with temperature and noise conditions that were not optimized. The data presented in the main text as well as in Fig. S5 and S6 were measured at reduced electron temperature, noise level as well as lower excitation current. Despite the unoptimized conditions, the data in Fig. S4 demonstrate that the results are in agreement with Landauer-Büttiker formalism.

Combining Eqs. (1) to (3), one obtains:

$$\frac{R_D - |R_D^-|}{2} = R_T. \tag{5}$$

The lower panel of Fig. S4(a) confirms the relation above by comparing $(R_D - |R_D^-|)/2$ with $R_T - R_{xx}$. In the quantum Hall regime, $R_{xx} = 0$ such that $(R_D + R_D^-)/2$ and $R_T - R_{xx}$ overlap. Comparing Eq. (1) and Eq. (3), one sees that:

$$R_T = R_D - R_{xy}. \tag{6}$$

This is also confirmed in Fig. S4(a).

Fig. S4(b) also shows that $R_T(I_{dc})$ and $R_D(I_{dc})$ both exhibit the zero bias peak. They share the same peak height and width, which are essential in the fit for determining both e^* and g. We illustrate this by vertically shifting the curve fitted to $R_D(I_{dc})$ to overlap with the data of $R_T(I_{dc})$.

EXTENDED DATA

We show in Fig. S5 and S6 the fitting and error analysis of tunneling peaks for different degrees of imbalance between the top and bottom layer recorded during a second cool-down and for a second quantum point contact.

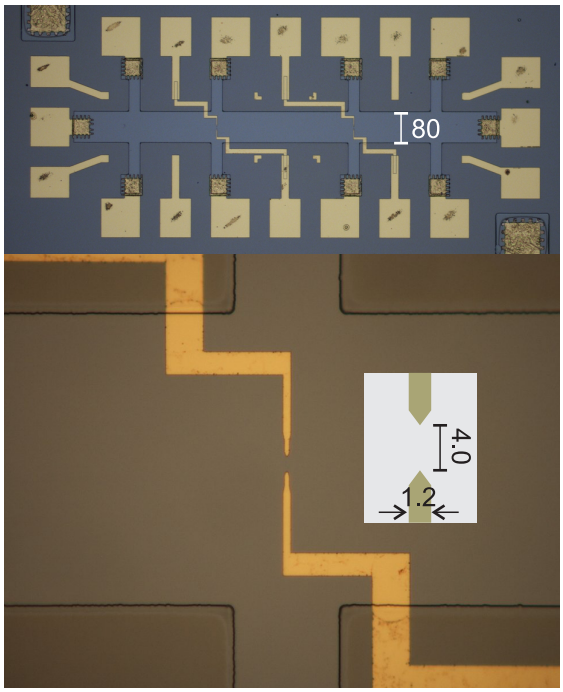

FIG. S1. Optical images of the patterned GaAs bilayer. The inset illustrates the design of the quantum point contact. Indicated lengths are in μm.

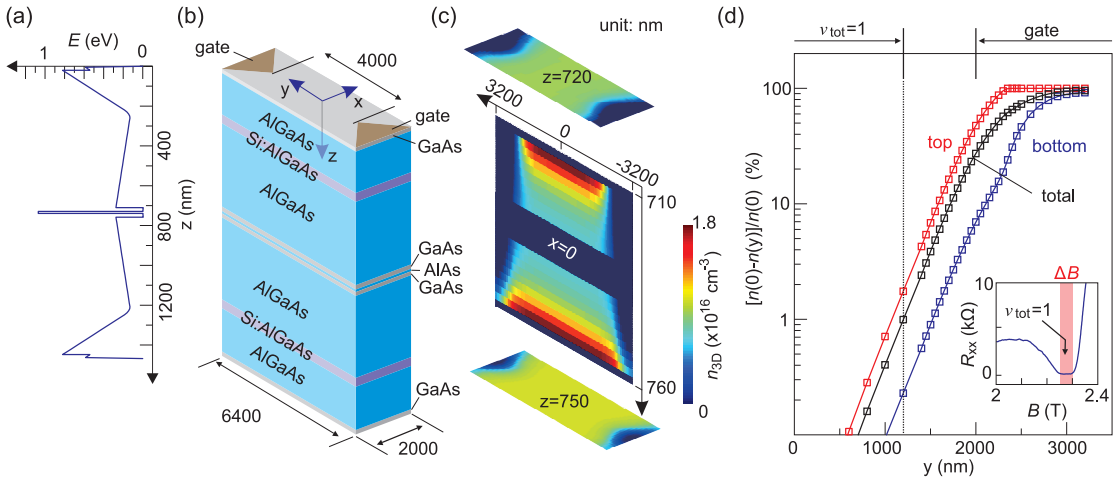

FIG. S2. Simulation of the quantum point contact (QPC) in the bilayer. (a) Conduction band profile at the center of the QPC ($x = 0, y = 0$). (b) GaAs double quantum well heterostructure used in the 3D simulation. Dimensions are in nm. (c) 2D cuts of the calculated 3D density distribution. The top and bottom color plot display the in-plane density variation inside the top and bottom quantum well, respectively. The panel in the middle shows the density distribution in the vertical direction. (d) Density variation from the center $y = 0$ to the edge $y = 3200$ nm. The plotted quantity is the relative density change. The density at the center of the QPC ($y = 0$) serves as the reference value. Red and blue squares represent the spatial dependence in the top and bottom quantum well. Black squares correspond the spatial dependence of the total density. The inset illustrates the magnetic field range over which the $\nu_{tot} = 1$ quantum Hall state is observed for the balanced case.

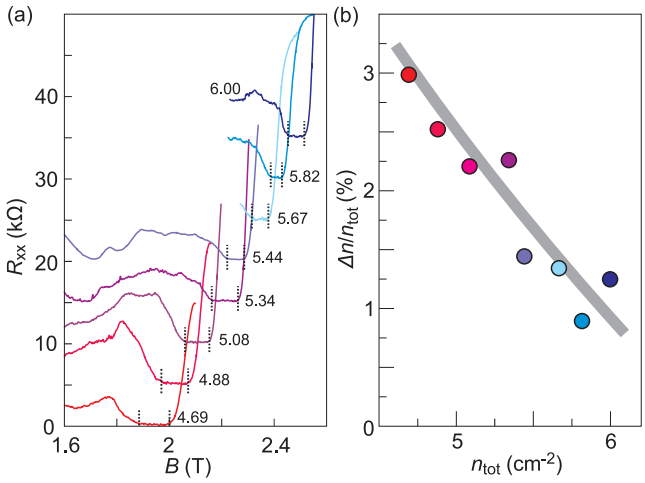

FIG. S3. (a) Longitudinal resistance measured around the $\nu_{tot} = 1$ state for different values of the total density. The curves have been recorded for increasing back gate voltages from 0.9 V (bottom trace) to 1.25 V (trace at the top) with a voltage step of 0.05 V. They are vertically offset for clarity. The number near each curve is the total density in units of $\times 10^{10}$ cm^{-2}. Dotted vertical bars demarcate the quantum Hall plateau/minimum. The distance between the vertical bars is referred to as ΔB and serves as a measure for the density change that can be tolerated before the $\nu_{tot} = 1$ state disappears, $\Delta n/n_{tot} = \Delta B/B_0$. (b) $\Delta n/n_{tot}$ as a function of the total density.

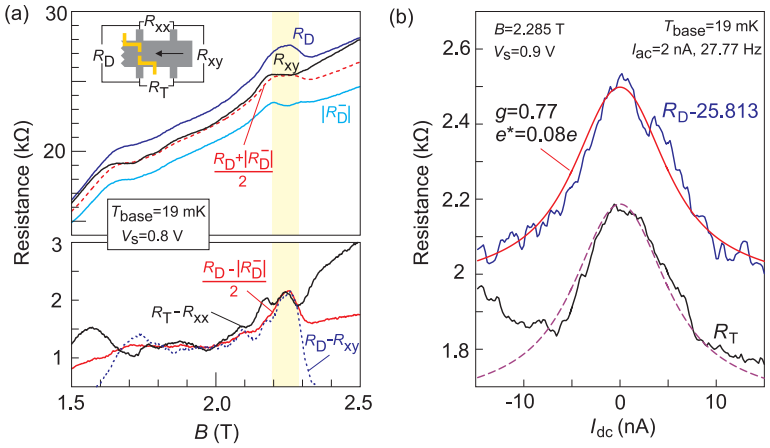

FIG. S4. (a) Magneto-resistance and Hall resistance traces. The inset explains the different quantities measured in the field sweep. R_D and R_D^- were obtained by sweeping B from 1.5 to 2.5 T and -1.5 to -2.5 T, respectively. (b) Current bias dependence of the longitudinal resistance (R_T) across the QPC as well as the diagonal resistance (R_D). Here R_D is subtracted by a constant of 25.813 kΩ to enable comparison. The solid red line is a fit to the $R_D(I_{dc})$ data. The electron temperature is assumed equal to 40 mK instead of the base temperature. This follows from the observation that the tunneling peak saturates at $T \leq 40$ mK in this dilution refrigerator. The dashed line is the same fit but shifted downward.

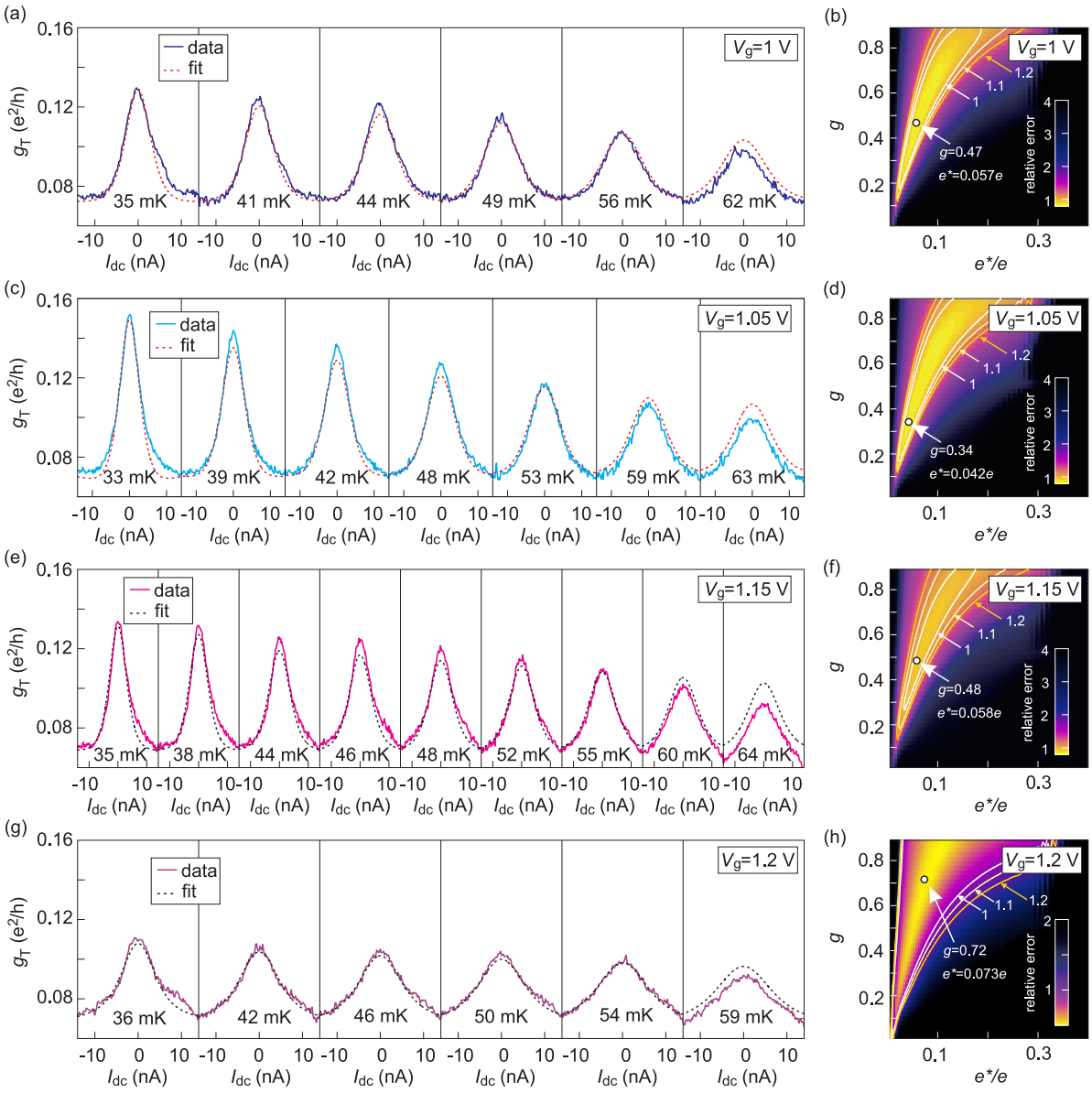

FIG. S5. (a)(c)(e)(g) Tunnel conductance (solid curve) as a function of dc current for different temperatures and four different degrees of imbalance between the top and bottom layer (V_g = 1, 1.05, 1.15, 1.2 V). Also shown are fit curves (dashed lines) generated with a single set of optimized fit parameters for all panels in the same row. These parameters are obtained by simultaneously fitting the formula for weak quasi-particle tunneling to all traces and minimizing the total error. (b)(d)(f)(h) Normalized fit error as a function of g and e^*/e. The circle marks the best fit point. The contours correspond to relative errors of 1, 1.1, and 1.2, as indicated by the arrows.

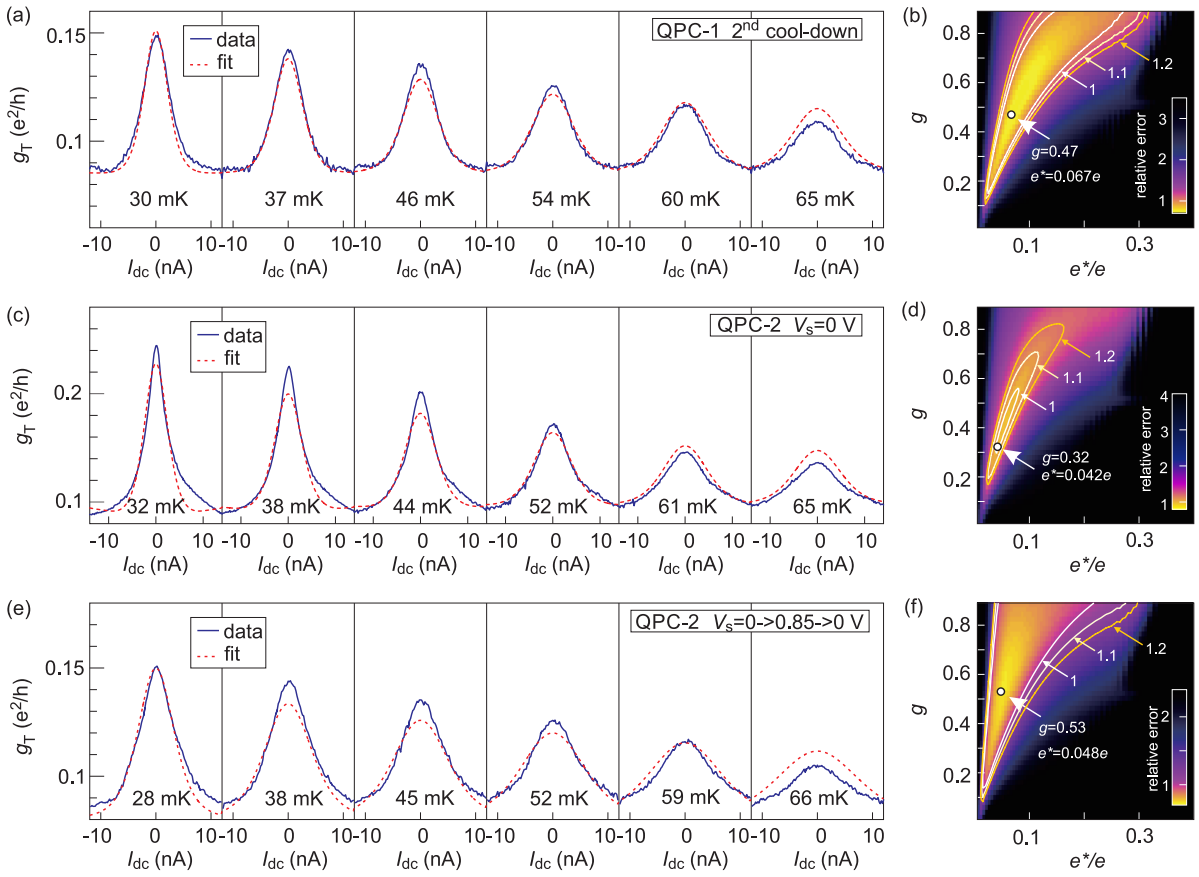

FIG. S6. (a)(c)(e) Tunnel conductance (solid curve) as a function of dc current at different temperatures for QPC-1 in another cool-down (different from the cool-downs discussed in the main text) and for QPC-2. Dashed lines are fits obtained with a single set of optimized fit parameters by simultaneously fitting the formula for weak quasi-particle tunneling for all traces and minimizing the error by simultaneously fitting the formula for weak quasi-particle tunneling for all traces and minimizing the total error. From (c) to (e), the split gate voltage was ramped up to 0.85 V and back. The positive gate voltage widens the QPC and reduces the tunneling peak. Due to some hysteresis at base temperatures, this electrostatic effect is preserved even after going back to 0 V. (b)(d)(f) Normalized fit error as a function of g and e^*/e. The circle marks the best fit point. The contours correspond to relative errors of 1, 1.1, and 1.2, as indicated by the arrows.